Matter Wave Sidebands from a Complex Potential with Temporal Helicity
Author(s): Stefan Bernet, Roland Abfalterer, Claudia Keller, Jorg Schmiedmayer and Anton Zeilinger
Source: *Proceedings: Mathematical, Physical and Engineering Sciences*, Vol. 455, No. 1984 (Apr. 8, 1999), pp. 1509-1520
Published by: The Royal Society
Stable URL: http://www.jstor.org/stable/53381
Accessed: 06/05/2014 06:42

Your use of the JSTOR archive indicates your acceptance of the Terms & Conditions of Use, available at http://www.jstor.org/page/info/about/policies/terms.jsp

JSTOR is a not-for-profit service that helps scholars, researchers, and students discover, use, and build upon a wide range of content in a trusted digital archive. We use information technology and tools to increase productivity and facilitate new forms of scholarship. For more information about JSTOR, please contact support@jstor.org.

The Royal Society is collaborating with JSTOR to digitize, preserve and extend access to *Proceedings: Mathematical, Physical and Engineering Sciences.*

http://www.jstor.org

This content downloaded from 130.132.123.28 on Tue, 6 May 2014 06:42:39 AM
All use subject to JSTOR Terms and Conditions

THE ROYAL SOCIETY

Matter wave sidebands from a complex potential with temporal helicity

BY STEFAN BERNET, ROLAND ABFALTERER, CLAUDIA KELLER, JÖRG SCHMIEDMAYER AND ANTON ZEILINGER

Institut für Experimentalphysik, Universität Innsbruck, Technikerstr. 25, A-6020 Innsbruck, Austria

Received 6 May 1998; accepted 27 July 1998

Atoms are diffracted at tailored time-modulated *complex* potential gratings made of light. Modulating both real and imaginary parts separately, the potential winds like a corkscrew in complex space. This temporal helicity induces energy transfers only in one single direction. As a result we present, to our knowledge, the first observation of asymmetric frequency sidebands of atomic matter waves.

Keywords: non-Hermitian potential; matter wave sideband; atom diffraction; diffraction asymmetry; complex potential; light crystal

1. Introduction

Potentials in quantum mechanics have to be Hermitian in order to guarantee unitarity of the Hamiltonian evolution. However, regarding only a subsystem which interacts with an otherwise non-interesting environment, it is possible to create a non-Hermitian potential, which can cause surprising effects within the subsystem. Using an open two-level system we experimentally realize a special case of a non-Hermitian potential, that is a time-dependent potential modulation of the form $V \sim \exp(\pm \mathrm{i}\omega t) + \text{const}$. We find that such a potential induces transitions between the energy eigenstates of a quantum system only in one direction, i.e. to higher or to lower energies. The direction depends on the sign of the exponent, which also defines the helicity of the temporal potential modulation in complex space. These directed transitions violate the inherent symmetry of any 'normal' (Hermitian) potential modulation: i.e. the transitions induce absorption and stimulated emission of a 'modulation quantum', $\hbar\omega$, with equal probability. Therefore, new possibilities arise, e.g. to create population inversion in a quantum system or to cool it to its ground state.

In practice, we create the complex potential modulation by using the interaction of an atom with on- and off-resonant light. This allows us to design a *complex* interaction potential between the atom and the light field, corresponding to a *complex* refractive index for the atomic matter wave. An atomic beam is scattered at a 'Bragg crystal' with such a *complex* index of refraction, which is modulated as a function of time. The 'crystal' consists of a thick standing light wave, which acts as a potential grating with an absorptive part (imaginary) and a refractive (real) part (Oberthaler *et al.* 1996), depending on the detuning of the light frequency from the atomic transition. As a result of the modulation, we observe frequency sideband generation of the atomic matter waves (Bernet *et al.* 1996*a*, *b*). The production of the sidebands is

© 1999 The Royal Society
TEX Paper

This content downloaded from 130.132.123.28 on Tue, 6 May 2014 06:42:39 AM
All use subject to JSTOR Terms and Conditions

due to resonant transitions of the atoms within the energy band structure of the light crystal, induced by the potential modulation. Using the specific atom–light interaction in our open system, we demonstrate how to tailor the desired helical potential modulation of the form $V \sim \exp(\pm i\omega t) + \text{const}$. This results in the first observation of asymmetric atomic matter wave sidebands. This asymmetry confirms that a 'one-way' transition of the atoms within the band structure of the light crystal has occurred, induced by the complex helicity of the potential modulation. The experimental realization of this strange effect exploits two recently developed techniques which will be described in the following sections: first the creation of *complex* light potentials for atoms, and second the diffraction behaviour of atoms at temporally modulated light potentials.

2. Complex light crystals for atoms

A light field acts as a potential for atoms if the light frequency, ω_L, is close to an atomic resonance, ω_{res}. Using an open atomic transition, where resonant excitation leads to a decay of the atoms to an undetected third state (ground state), the interaction potential becomes complex. Its spectral shape is described by a resonance line (Chudesnikov & Yakovlev 1991):

$$V(\omega_L) = \frac{\hbar {\Omega_R}^2}{\omega_{res} - \omega_L + \frac{1}{2}i\gamma}, \tag{2.1}$$

where γ is the linewidth of the transition to the undetected state and $\Omega_R = dE/\hbar$ is the Rabi frequency at resonance, depending on the light electric field E and the transition dipole moment d. The real and imaginary parts correspond to the real dipole interaction potential and to absorption, respectively. The absorption is due to the decay of the atoms to the undetected state. Such a potential gives rise to a complex index of refraction, $n \sim 1 - V/2E_{kin}$, for atoms with kinetic energy E_{kin}. Therefore, a *standing* light field represents a refractive index grating for atomic matter waves. We create our light gratings in front of a retro-reflection mirror by reflecting a collimated laser beam at the surface. Diffraction of atoms at such a light grating is possible in full analogy with the 'traditional' diffraction of light at material gratings. This has been shown in thin- and thick-grating (Bragg) (Gould *et al.* 1986) diffraction regimes, and for the diffraction behaviour at pure refractive index and absorptive 'light crystals' (Oberthaler *et al.* 1996) consisting of thick standing light waves.

According to equation (2.1) it is possible to produce an almost purely real potential using light which is far detuned on either side of the atomic resonance, or to produce a purely imaginary potential with resonant light. In order to design our time-orientated complex potential, we use the possibility of overlapping two different light crystals by superposing two independent laser beams at a beamsplitter cube. If the potentials of the two light fields are small enough to exclude saturation effects, the resulting potential is just the sum of the two individual potentials†. Since the two lasers frequencies are closely adjacent (maximal difference 120 MHz), the two standing light waves lie exactly on top of each other in front of the mirror surface. By modulating the intensity of the two laser beams independently with the same rate ω_M, but

† Note that internal coherences in the atom excitation process play no role because two independent lasers are used to generate the two overlapping light crystals.

This content downloaded from 130.132.123.28 on Tue, 6 May 2014 06:42:39 AM
All use subject to JSTOR Terms and Conditions

an adjustable relative phase φ_M, we can create a spatially and temporally periodic light-crystal potential $V(x,t)$ of the form

$$V(x,t) = [V_1(1+\cos(\omega_M t)) + V_2(1+\cos(\omega_M t + \varphi_M))][1+\cos(Gx)], \tag{2.2}$$

where G is the common grating vector of the two overlapping light crystals, and V_1, V_2 are the amplitudes of the potentials created by the two light beams. In our experiments we can choose the amplitudes to be negative, positive or imaginary by adjusting the respective laser frequencies according to equation (2.1). The spatial part of the potential represents the standing light intensity grating, which is temporally modulated by the time-dependent factors.

3. Bragg diffraction of atoms at modulated potentials

The next step is to recapitulate how such a time-modulated potential affects atomic diffraction. It has been shown (Bernet *et al.* 1996*a*, *b*) that a 'normal' intensity-modulated light crystal produces frequency sidebands, which are *symmetrically* offset to higher and lower energies by multiples of the modulation rate. In analogy with light optics, the ability of a time-dependent potential to create a sideband with a certain frequency offset depends only on the corresponding Fourier coefficient of the temporal modulation. In the case of low sideband production efficiencies, the intensities of frequency up-shifted (P_{up}), frequency down-shifted (P_{down}) and unshifted atoms (P_0) should be proportional to the absolute squares of these Fourier coefficients†:

$$P_0 \sim |V_1 + V_2|^2, \qquad P_{up,down} \sim |\tfrac{1}{2}(V_1 + V_2 e^{\pm i\varphi_M})|^2. \tag{3.1}$$

Since there are three adjustable parameters V_1, V_2 (real or imaginary) and φ_M, these relations imply that the intensity can be redistributed arbitrarily between the three sidebands.

Now the question of how to identify the frequencies of the atomic sidebands arises. Fortunately, this has already been solved (Bernet *et al.* 1996*a*, *b*). It has been demonstrated that atomic sidebands produced by diffraction at a time-modulated light crystal appear as new Bragg peaks at new incidence angles.

This behaviour can be explained in an Ewald construction (figure 1) for first-order scattering processes. Due to momentum conservation, incident and diffracted wavevectors (k_{in} and k_{out}) always have to be connected by a grating vector (G). Additionally, in static scattering (figure 1*a*) the energy is conserved, corresponding to conservation of the lengths of incident and scattered wavevectors. Thus, the pair of allowed incident, k_{in}, and scattered wavevectors, k_{out}, forms a symmetric triangle with the grating vector G. Since the direction and length of a grating vector in an extended crystal are sharply defined, there are only discrete Bragg angles for a given incident wavevector.

In the case of a periodically oscillating crystal (modulation rate ω_M) the grating vector still remains sharply defined. However, for long enough interaction times ($\tau \gg 1/\omega_M$) the temporal modulation allows for a quantized energy exchange between

† In analogy with spatial diffraction, these relations apply only for low efficiencies of diffraction or sideband production. However, the statement that each sideband is only influenced by its corresponding Fourier coefficient usually remains valid. For larger efficiencies a deviation from the quadratic dependence is expected.

This content downloaded from 130.132.123.28 on Tue, 6 May 2014 06:42:39 AM
All use subject to JSTOR Terms and Conditions

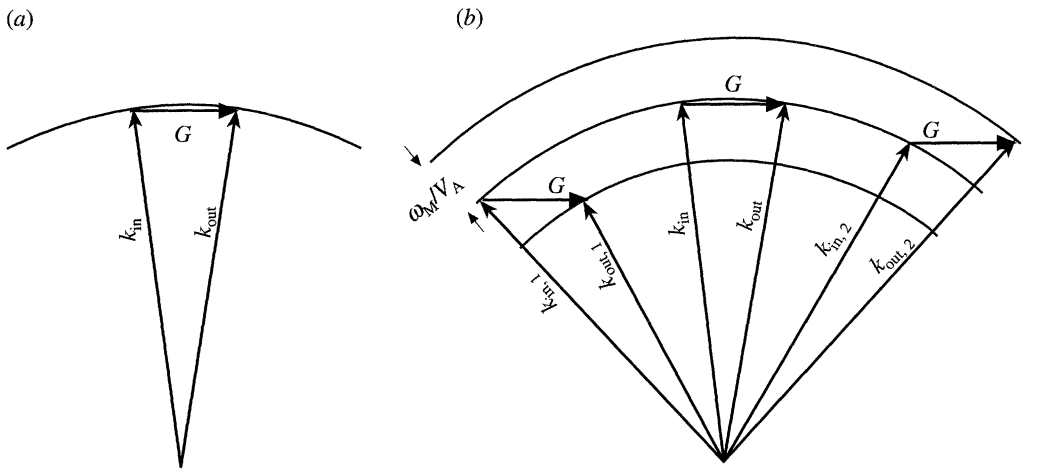

Figure 1. Ewald construction for first-order diffraction at a static crystal (a) and at a periodically modulated crystal (b). Due to energy and momentum conservation in the case of static Bragg diffraction (a), the pair of incident and diffracted wavevectors, k_{in} and k_{out}, forms a symmetric triangle with the grating vector G. For a given absolute value of the atomic velocity v_{A} and a certain diffraction direction, there is only one incidence angle allowed. In (b) the periodic modulation of the crystal additionally enables a quantized energy exchange of a modulation quantum $\pm\hbar\omega_{\mathrm{M}}$. Therefore the length of the scattered wavevector can change by approximately $(\pm\omega_{\mathrm{M}}/v_{\mathrm{A}})$. For diffraction in the same order as in (a) there are now two new possible pairs ($k_{\mathrm{in},1} \rightarrow k_{\mathrm{out},1}$ and $k_{\mathrm{in},2} \rightarrow k_{\mathrm{out},2}$) of incident and diffracted wavevectors, in addition to the original pair of (a). For small energy shifts and small grating vectors with respect to the atomic wavevector, the angular offset of the two new incidence angles from the static Bragg angle (indicated in the figure) is approximately symmetric, and the total scattering angle does not change. In our experiments, the direction of the atomic beam is kept fixed in the laboratory, whereas the incidence direction at the crystal is changed by rotating the crystal. Therefore, first-order Bragg diffraction at a given direction now appears at the static Bragg angle, and at the two almost symmetrically displaced new crystal angles, resulting in energetically up- and down-shifted atoms. The corresponding scattering angles of the three cases are approximately equal.

the crystal and incident wave of $\pm\hbar\omega_{\mathrm{M}}$, i.e. the de Broglie frequency of the scattered atoms changes exactly by $\pm\omega_{\mathrm{M}}$. This holds for all kinds of potential modulations which supply time-dependent Fourier contributions of frequency ω_{M}, e.g. for intensity- or phase-modulated (spatially vibrating) crystals. In the Ewald construction (figure 1b) this leads to a change in the length of the scattered wavevector of $(\pm\omega_{\mathrm{M}}/v_{\mathrm{A}})$, where v_{A} is the velocity of the atoms (the approximation holds for small modulation frequencies with respect to the de Broglie frequency of the incident atoms). In this case the tips of incident and scattered wavevectors are located on concentric circles with different radii. Normally, both absorption and emission of a modulation quantum $\hbar\omega_{\mathrm{M}}$ are possible, resulting in two new Ewald circles for frequency up- and down-shifting diffraction, respectively. Therefore, for diffraction in a given direction, two new pairs of incident and scattered wavevectors are allowed ($k_{\mathrm{in},1} \rightarrow k_{\mathrm{out},1}$ and $k_{\mathrm{in},2} \rightarrow k_{\mathrm{out},2}$), each connected by the same grating vector G. The corresponding incidence angles are located symmetrically around the static Bragg angle. In our experiment the Bragg scattering angles are of the order of 20 μrad. In

This content downloaded from 130.132.123.28 on Tue, 6 May 2014 06:42:39 AM
All use subject to JSTOR Terms and Conditions

this case the separation between the incidence angles of static and frequency-shifted scattering is proportional to the corresponding frequency shift of the atoms, and thus to the modulation rate (Bernet *et al.* 1996*a*, *b*). In particular, the sign of the frequency shift corresponds to the direction of the angular deviation. Thus, a modulated Bragg crystal represents both a sideband synthesizer and an analyser at the same time. This is an important prerequisite for our experiment, allowing for the identification of atomic frequency sidebands as Bragg peaks at the new incidence angles.

4. Experiment

In our experiment (our experimental set-up is described in more detail in Batelaan *et al.* (1997)) (figure 2), we use argon atoms that are excited by a DC gas discharge to a metastable state (lifetime *ca.* 30 s). After excitation the thermal atomic beam ($v = 700\,\mathrm{m\,s^{-1}} \pm 60\%$) is collimated (less than 6 μrad) by two slits (10 μm and 5 μm) separated by a distance of 1.4 m. Then the atoms pass a thick (4 cm) standing light wave, created by retro-reflection of two overlapped collimated laser beams at a mirror which can be tilted by a piezo-actuator. The grating constant (401 nm) corresponds to one half of the optical wavelength (801.7 nm). Atoms are diffracted by this one-dimensional Bragg crystal if their incidence angle corresponds to a Bragg angle ($\Theta_\mathrm{B} = \pm 18\,\mu\mathrm{rad}$). Another 1.4 m downstream a third 10 μm slit selects only first-order diffracted atoms, which are then counted by our 'channeltron' detector as a function of their incidence angle at the light crystal. The channeltron registers only metastable atoms, whereas ground-state atoms remain undetected. This gives us the chance to realize an imaginary potential by resonant excitation with laser light at 801.7 nm ($1s_5 \rightarrow 2p_8$), which leads to a relaxation of the atoms to the non-detected ground state (see inset of figure 2). This corresponds to absorption and supplies the Lorentzian imaginary part of the potential in equation (2.1).

The Bragg crystal is produced by superposing light from two lasers—the frequencies are locked independently on-resonance (imaginary potential) or far detuned (by $\pm 60\,\mathrm{MHz} \approx \pm 10\gamma$) on either side of the absorption line (positive or negative potential). The corresponding two light crystals are situated exactly on top of each other. Typical light intensities were *ca.* $0.08\,\mathrm{mW\,cm^{-2}}$ for the absorptive crystal and $1.5\,\mathrm{mW\,cm^{-2}}$ for the light field detuned by 60 MHz (*ca.* 10 linewidths). Thus the intensities were small with respect to the saturation intensity of $2.2\,\mathrm{mW\,cm^{-2}}$ for resonant excitation. Modulating the intensity of the two lasers, by switching two acousto-optic modulators (figure 2) in the two individual beams on and off with well-defined relative temporal phase φ_M, allows the creation of the general time-dependent potential variations mentioned previously (equation (2.2)).

We first present diffraction experiments at such a light crystal with both components far detuned (real potentials) and modulated with a frequency of $\omega_\mathrm{M} = 2\pi \times 100\,\mathrm{kHz}$. During its passage through the crystal each atom experiences about six switching cycles. The absolute values of the two potentials were equalized ($|V_1| \cong |V_2| =: V_0$) by adjusting the light intensities of the two individual gratings for approximately the same diffraction efficiencies (*ca.* 20%). In figure 3 the intensity of atoms scattered at the first diffraction order is displayed as a function of the atomic incidence angle at the light crystal (mirror angle). The centre of each plot corresponds

This content downloaded from 130.132.123.28 on Tue, 6 May 2014 06:42:39 AM
All use subject to JSTOR Terms and Conditions

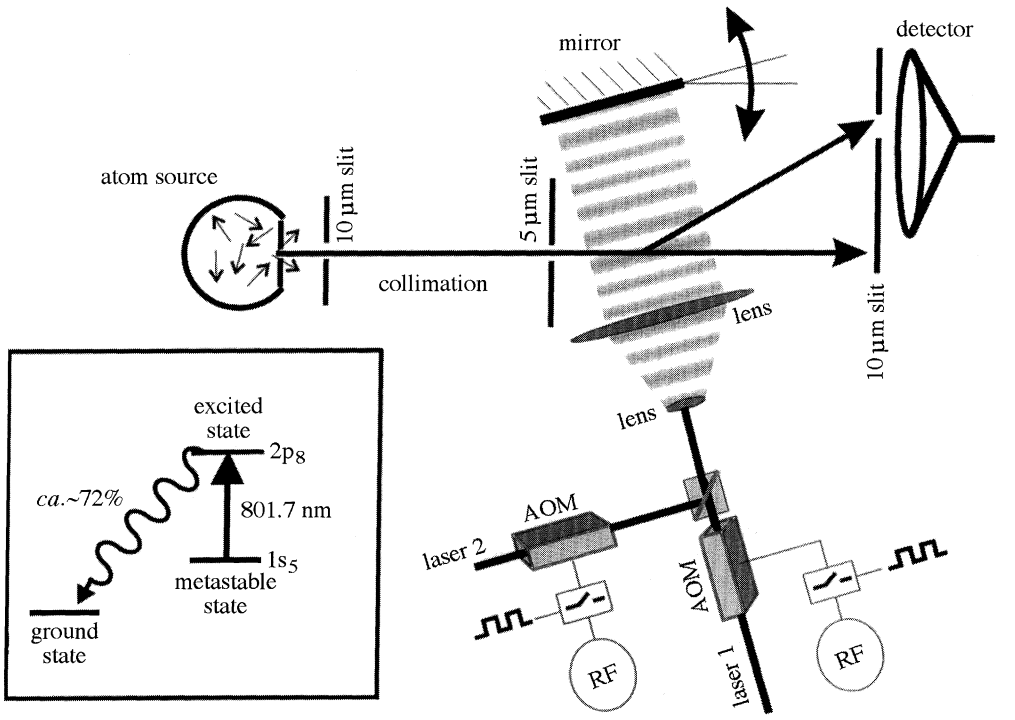

Figure 2. Experimental set-up (not to scale). A collimated thermal beam of metastable argon atoms crosses a standing light wave. First-order diffracted atoms are registered by a channeltron detector as a function of their incidence angle at the light crystal (mirror angle). The inset shows the levels involved in the 801.7 nm transition of metastable argon.

to the static Bragg angle. As explained above, atoms diffracted at other incidence angles are frequency up- or down-shifted, depending on the sign of the angular offset.

In figure 3*a* both lasers were red detuned ($V_1 = V_2 = -V_0$) with respect to the absorption line, and both were periodically switched on and off simultaneously ($\varphi_M = 0$, see inset). The situation corresponds to one single intensity-modulated laser (Bernet *et al.* 1996*a*, *b*), and the results are identical: one peak at the static Bragg angle (centre) and two smaller symmetrically located sidepeaks consisting of energetically up- and down-shifted atoms. The intensity ratio between the peaks is approximately 1:4:1 and thus agrees with the predictions of equations (3.1).

In figure 3*b* both lasers were red detuned as before ($V_1 = V_2 = -V_0$), but now switched with a relative phase of $\varphi_M = \pi$, i.e. alternately (see inset). In effect, the atoms see a time-independent red-detuned light crystal, and the situation corresponds to the case of normal static Bragg diffraction. Consequently, atoms are only scattered at the static Bragg angle (one peak at the centre).

Figure 3*c* corresponds to the case where the two lasers are detuned on different sides of the resonance frequency ($V_1 = -V_2 = -V_0$) with equal switching phase ($\varphi_M = 0$). The total potential is always zero and no atoms are diffracted at all.

In figure 3*d* the two lasers are still detuned on different sides of the resonance frequency, but now they are switched alternately ($\varphi_M = \pi$). This corresponds to

This content downloaded from 130.132.123.28 on Tue, 6 May 2014 06:42:39 AM
All use subject to JSTOR Terms and Conditions

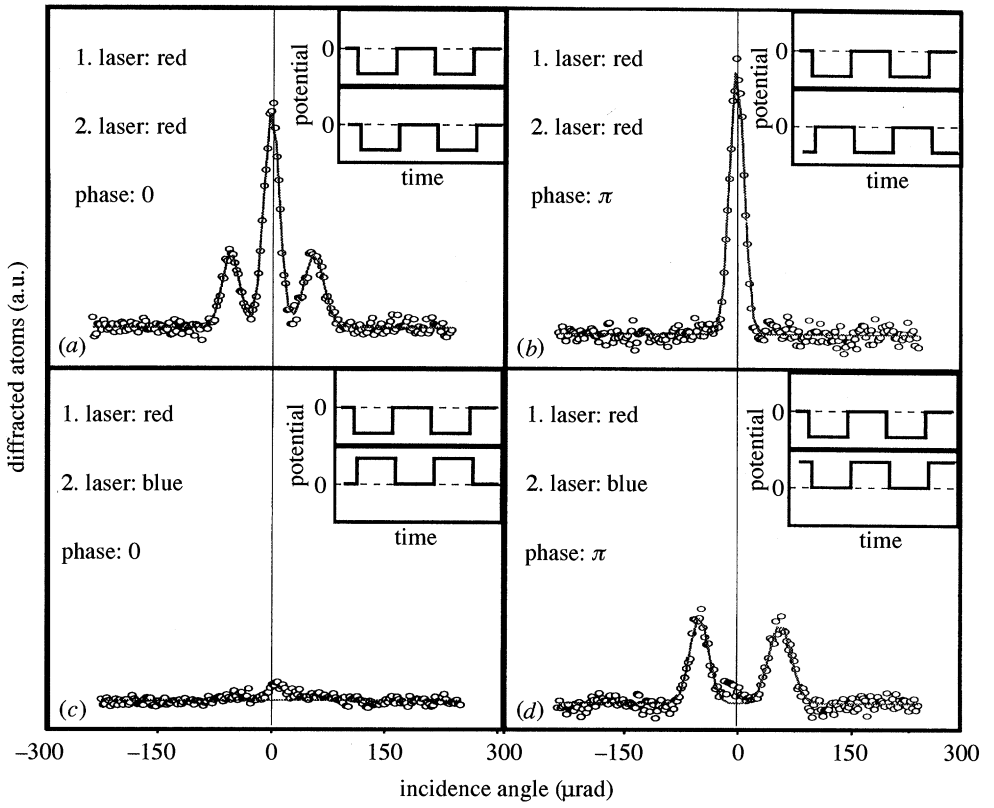

Figure 3. Dependence of the matter wave sideband generation on the Fourier composition of a *real* potential modulation. Diffracted atoms are plotted as a function of the atomic incidence angle for different realizations of a Hermitian time-modulated potential. The centre of each plot corresponds to the static Bragg angle. Peaks at other positions correspond to frequency-shifted atoms. The insets show the respective potential modulations of the two spatially coinciding light crystals. The situation in (*a*), where both lasers are red detuned and switched simultaneously, corresponds effectively to one intensity-modulated light crystal resulting in both a static Bragg peak and two sideband peaks. In (*b*) the two red-detuned lasers are switched alternately. Therefore, the effective crystal is time-independent, thus giving only the static peak. In (*c*) the two lasers are detuned on different sides of the atomic resonance, and switched simultaneously. The corresponding two potentials completely cancel each other at any time, and no diffraction results. Finally, in (*d*) the two lasers with opposite detunings are switched alternately. Therefore, the time average of the potential vanishes, although a time-modulated contribution as in (*a*) is created. Consequently, the diffracted atoms exhibit the two sidebands, but the static Bragg peak at the centre is suppressed.

the interesting situation where the atoms see a crystal jumping between a positive and a negative potential. The *time average* of the potential completely vanishes ($V_1+V_2=0$), although the *time-dependent* contributions are the same as in figure 3*a*. Therefore the static Bragg peak is completely suppressed, whereas the frequency sidebands still arise.

These experiments demonstrate that the efficiency of frequency sideband generation depends on the Fourier composition of the temporal potential modulation, in a

This content downloaded from 130.132.123.28 on Tue, 6 May 2014 06:42:39 AM
All use subject to JSTOR Terms and Conditions

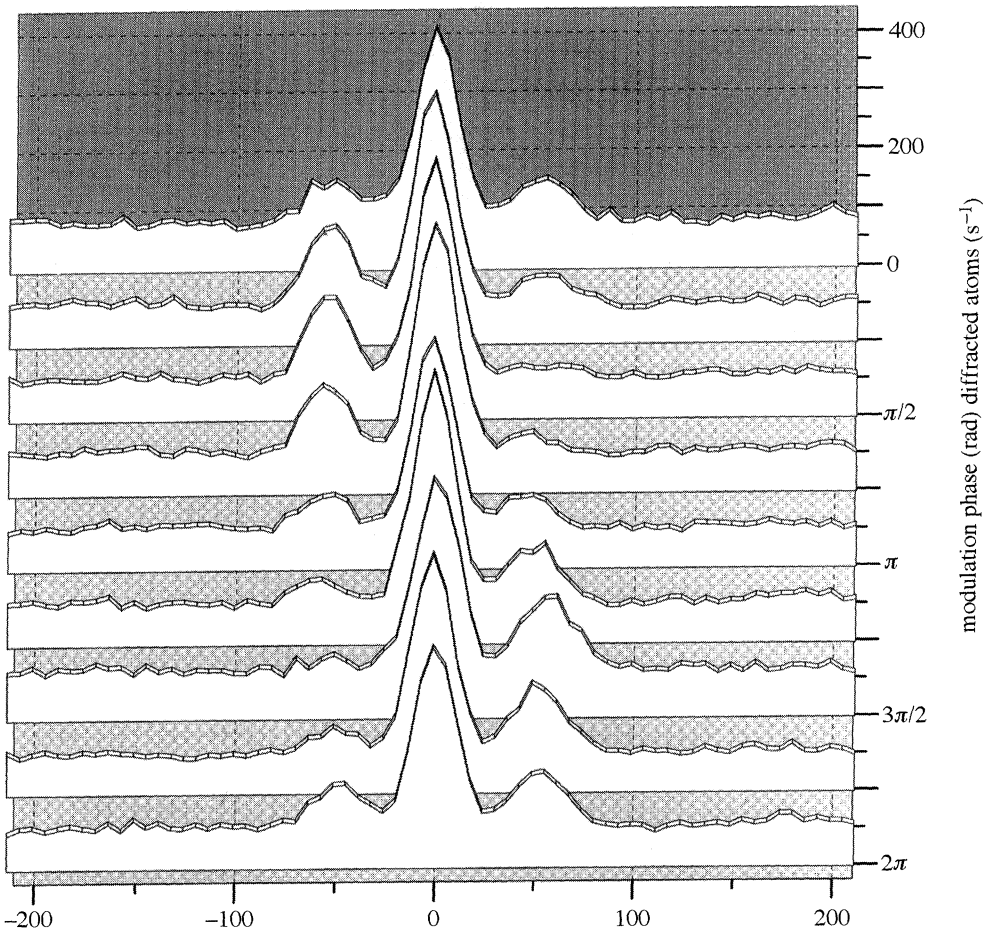

Figure 4. Asymmetric matter wave sidebands created by a non-Hermitian potential modulation with an orientation in time. The first-order diffracted atoms are plotted as a function of their incidence angle for different temporal phases in the modulation of a resonant and an off-resonant laser. The centre of each plot corresponds to the static Bragg angle. The sidepeaks consist of atoms whose de Broglie frequency is shifted by the modulation rate $\omega_{\mathrm{M}} = 100$ kHz. The sign of the frequency shift is determined by the sign of the angular offset. Depending on the temporal phase, different types of non-Hermitian potential modulations result, including the extreme cases of $V \sim \exp(\pm \mathrm{i}\omega_{\mathrm{M}} t) + \mathrm{const.}$ at modulation phases of $\frac{1}{2}\pi$ and $\frac{3}{2}\pi$. In these cases an almost complete asymmetry of the frequency sideband generation is obtained.

similar way to spatial scattering where the diffraction efficiency of a crystal depends on the Fourier components of the spatial potential modulation. This model also describes non-trivial situations, as in figure 3*d*. In the following it will be applied even to the case of non-Hermitian potentials.

In the next experiments we build our general time-modulated complex potentials, including the special cases $V \sim \mathrm{e}^{\pm \mathrm{i}\omega_{\mathrm{M}} t} + \mathrm{const.}$ The difference is that now one of the lasers is tuned on resonance (absorptive crystal, imaginary potential), whereas the

This content downloaded from 130.132.123.28 on Tue, 6 May 2014 06:42:39 AM
All use subject to JSTOR Terms and Conditions

other laser remains red detuned (refractive crystal, negative potential). After adjusting the laser intensities of the two individual subcrystals for equal relative diffraction efficiencies, we get $V_1 = -\mathrm{i}V_2 = -V_0$. Each graph in the series of figure 4 corresponds to a different relative modulation phase, φ_M, of the two lasers, changing between 0 and 2π in steps of $\frac{1}{4}\pi$. In the cases where the switching of the two lasers was performed simultaneously ($\varphi_\mathrm{M} = 0$, first and last graph) or alternately ($\varphi_\mathrm{M} = \pi$, middle graph), the results are still symmetric, with one central Bragg peak and two sidepeaks. According to equations (3.1), the peak ratios should be 1:4:1. All other plots show an asymmetric distribution of the sidebands as expected from equations (3.1). The extreme situations $\varphi_\mathrm{M} = \frac{1}{2}\pi$ and $\varphi_\mathrm{M} = \frac{3}{2}\pi$ result in a completely asymmetric sideband production. As expected from equations (3.1) the intensity of the asymmetric sideband is approximately doubled with respect to the symmetric situations. There the time-dependent part of the corresponding potential modulation becomes $V(t) \sim \mathrm{e}^{\pm\mathrm{i}\omega_\mathrm{M}t}$, corresponding to a helix in complex space.

A more detailed evaluation of the sidepeak intensities is plotted in figure 5. There, the relative efficiencies of sideband generation are determined from the integral intensities of the sidepeaks, normalized by the intensity of the static Bragg peak. The graph clearly shows the opposite behaviour of frequency up-shifted and frequency down-shifted atoms. As expected from equations (3.1), the efficiencies of sideband production vary sinusoidally as a function of the temporal modulation phase between the absorptive and the off-resonant light crystals.

These experiments demonstrate, to our knowledge, for the first time, an asymmetric sideband production of matter waves. The discussion in the next section will show that this corresponds to a directed energy transfer induced by a resonant excitation, which violates the usual symmetry between absorption and stimulated emission.

5. Discussion

Interestingly, our sideband generation can also be interpreted as a transition of the atoms between the energy bands of the light crystal, induced by the time-modulated potential. In figure 6 these eigenenergies are plotted as a function of the atomic wavevector component $k_{A\|}$ parallel to the grating vector G (Dahan *et al.* 1996; Wilkinson *et al.* 1996). Thus, if all atomic wavevectors are assumed to have the same length (momentum), the $k_{A\|}$-axis corresponds to the incidence angle of the atoms at the crystal. The dashed parabola corresponds to the dispersion of a free atom outside the crystal. At the crystal boundary an originally free atom is coupled into the particular band which matches its free (kinetic) energy parabola. Thus, at most incidence angles the atoms occupy only one crystal eigenstate. Since eigenstates do not change in time, these atoms are coupled out at the end of the crystal in the same way as those coupled in, and no diffraction is possible. Simultaneous population of two (adjacent) bands occurs only at the band gaps, for example at position 'a' in figure 6, followed by a time evolution and a 'normal' static Bragg diffraction process.

However, in a time-modulated crystal, diffraction can also be observed at other incidence angles, where atoms 'normally' should occupy only one crystal band. The explanation in this picture is that these atoms can be excited resonantly into a superposition of two bands if the crystal is modulated with the corresponding frequency difference (e.g. arrows b or c in figure 6). This results in Bragg diffraction of frequency-shifted matter waves. A calculation of the modulation rate as a function

This content downloaded from 130.132.123.28 on Tue, 6 May 2014 06:42:39 AM
All use subject to JSTOR Terms and Conditions

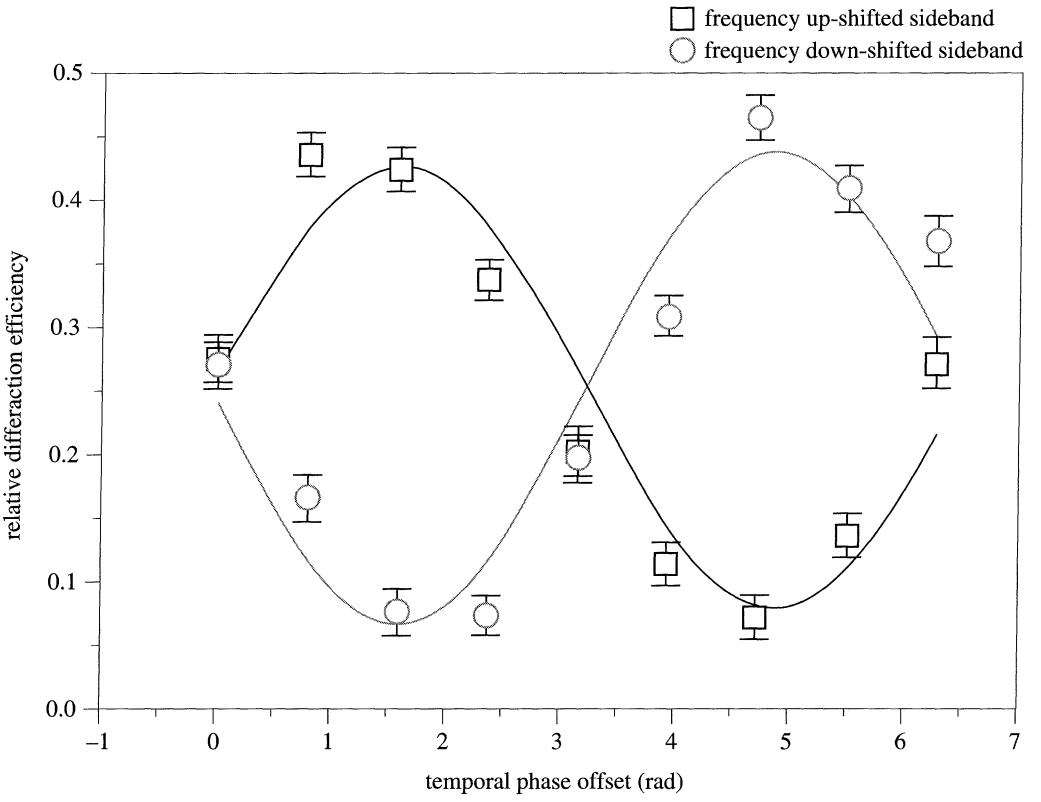

Figure 5. Relative efficiencies of the generation of frequency up-shifted and down-shifted sidebands as a function of the relative temporal oscillation phase between the absorptive and the off-resonant light crystals. The data points are fits of the sidepeak intensities in figure 4.

of the incidence angle yields the same results as the generalized Ewald construction sketched above. Obviously, resonant transitions to higher (e.g. arrow b) and lower bands (e.g. arrow c) are arranged symmetrically around the static Bragg angles (e.g. position a), which explains the symmetric distribution of the sideband peaks in 'conventionally' modulated crystals (Bernet *et al.* 1996*a*, *b*). On the other hand, the asymmetric sidebands of our present experiment suggest the presence of a *different* type of perturbation, which induces resonant transitions only in *one* direction. For example, although the modulation may induce a transition (b) to a higher energy band, there is no transition to an equally spaced lower energy band under incidence condition (c). The ability of such helical complex potentials to produce lop-sided transitions might imply applications like cooling of atoms in optical lattices, or, on the contrary, creating population inversion. However, in our present experiment this is not possible since we do not realize the pure situation $V \sim \mathrm{e}^{\mathrm{i}\omega_{\mathrm{M}}t}$. Instead we have to consider a constant imaginary contribution which causes absorption. Nevertheless, extending our experiment to a system where repumping of ground-state atoms is possible might solve this problem and realize the pure case.

It is also interesting to note that our asymmetric sideband creation has a spatial analogue, which is not trivial since the Schrödinger equation is unsymmetric with respect to temporal and spatial coordinates. It consists of a violation of the

This content downloaded from 130.132.123.28 on Tue, 6 May 2014 06:42:39 AM
All use subject to JSTOR Terms and Conditions

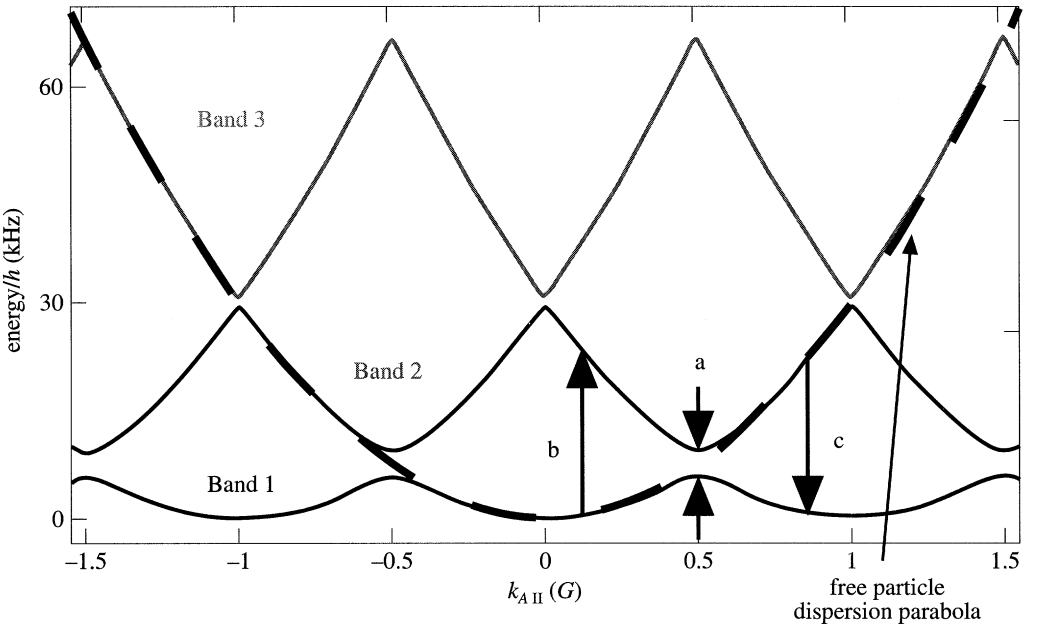

Figure 6. Band structure of atomic matter waves in a one-dimensional light crystal. Transitions within the band structure (arrows b and c) are induced by a resonant perturbation and result in new Bragg peaks of frequency-shifted atoms.

typical diffraction symmetry with respect to conjugate diffraction orders, known as Friedel's law, as recently observed for atoms diffracted at a complex light crystal (Keller *et al.* 1997). There, the crystal was a superposition of two *spatially* displaced absorptive and refractive light gratings. This resulted in a *spatial* helicity of the complex crystal potential $V(x) \sim \mathrm{e}^{\pm \mathrm{i}Gx}$, which permitted a transfer of a grating momentum $\pm\hbar G$ (diffraction) only in one direction (Berry 1998). Similarly, our helicity in the time domain $V(t) \sim \mathrm{e}^{\pm \mathrm{i}\omega_{\mathrm{M}}t}$ induces energy transfers only in one direction. By combining the two effects it now becomes feasible to produce a light potential $V(x,t) \sim \mathrm{e}^{\pm \mathrm{i}Gx \pm \mathrm{i}\omega_{\mathrm{M}}t}$ which has the appearance of an artificial travelling de Broglie wave. Bragg diffraction of atoms at such a potential implies the alternative description of an elastic collision of two de Broglie particles. We expect interesting new insights in quantum scattering from proceeding investigations of such time-modulated *complex* potentials.

This work was supported by the Austrian Science Foundation (FWF), project number S6504, and by the European Union TMR grant ERB FMRX-CT96-0002.

References

Batelaan, H., Bernet, S., Oberthaler, M. K., Rasel, E., Schmiedmayer, J. & Zeilinger, A. 1997 Classical and quantum atom fringes. In *Atom interferometry* (ed. P. E. Berman), pp. 85–120. New York: Academic.

Bernet, S., Oberthaler, M. K., Abfalterer, R., Schmiedmayer, J. & Zeilinger, A. 1996*a* Coherent frequency shift of atomic matter waves. *Phys. Rev. Lett.* **77**, 5160–5163.

Bernet, S., Oberthaler, M. K., Abfalterer, R., Schmiedmayer, J. & Zeilinger, A. 1996*b* Modulation of atomic de Broglie waves using Bragg diffraction. *Quantum Semiclass. Opt.* **8**, 497–509.

This content downloaded from 130.132.123.28 on Tue, 6 May 2014 06:42:39 AM
All use subject to JSTOR Terms and Conditions

Berry, M. V. 1998 Lop-sided diffraction by absorbing crystals. *J. Phys.* A **31**, 3493–3502.

Chudesnikov, D. O. & Yakovlev, V. P. 1991 *Laser Phys.* **1**, 110.

Dahan, M. B., Peik, E., Reichel, J., Castin, Y. & Salomon, C. 1996 *Phys. Rev. Lett.* **76**, 4508.

Gould, P. L., Ruff, G. A. & Pritchard, D. E. 1986 *Phys. Rev. Lett.* **56**, 827.

Keller, C., Abfalterer, R., Bernet, S., Oberthaler, M. K., Schmiedmayer, J. & Zeilinger, A. 1997 *Phys. Rev. Lett.* **79**, 3327.

Oberthaler, M. K., Abfalterer, R., Bernet, S., Schmiedmayer, J. & Zeilinger, A. 1996 Atom waves in crystals of light. *Phys. Rev. Lett.* **77**, 4980–4983.

Wilkinson, S. R., Bharucha, C. F., Madison, K. W., Quian Niu & Raizen, M. G. 1996 *Phys. Rev. Lett.* **76**, 4512.

This content downloaded from 130.132.123.28 on Tue, 6 May 2014 06:42:39 AM
All use subject to JSTOR Terms and Conditions